

The influence of van der Waals forces on a bubble moving in a tube

Naima H. Hammoud*

*Program in Applied and Computational Mathematics,
Princeton University, Princeton, NJ 08544, USA*

Philippe H. Trinh

*Oxford Centre for Industrial and Applied Mathematics,
Mathematical Institute, University of Oxford, Oxford OX2 6GG, UK*

Peter D. Howell

*Oxford Centre for Industrial and Applied Mathematics,
Mathematical Institute, University of Oxford, Oxford OX2 6GG, UK*

Howard A. Stone

*Department of Mechanical and Aerospace Engineering,
Princeton University, Princeton, NJ 08544, USA*

(Dated: May 11, 2017)

We present a theoretical study of the unsteady thin-film dynamics of a long bubble of negligible viscosity that advances at a uniform speed in a cylindrical capillary tube. The bubble displaces a viscous, nonwetting fluid, creating a thin film between its interface and the tube walls. The film is considered thin enough that intermolecular forces in the form of van der Waals attractions are significant and thin-film rupture is possible. In the case of negligible intermolecular forces, a steady-state solution exists where a film of uniform thickness is deposited in the annular region between the bubble interface and the tube walls. However, once intermolecular interactions are important, the interface is perturbed out of its steady state and either (i) the perturbation grows sufficiently before reaching the rear meniscus of the bubble such that rupture occurs; or (ii) the perturbation remains small due to weak intermolecular forces until it leaves the bubble interface through the rear meniscus. We obtain, both numerically and asymptotically, the time-scale over which rupture occurs, and thus, we find a critical capillary number, depending on the bubble length and the strength of the intermolecular forces, below which the film is predicted to rupture.

* nhammoud@princeton.edu

I. INTRODUCTION

When a bubble of negligible viscosity advances in a circular tube filled with a wetting, viscous fluid, a uniform thin film is deposited between the bubble interface and the tube walls. This setup was first studied experimentally by Fairbrother & Stubbs [1] and Taylor [2]. A theoretical framework using the lubrication approximation was proposed by Bretherton [3], who found that the thickness of the film varies as a two-thirds power law with the capillary number, which measures the relative strength of viscous to surface tension forces. Through comparisons with both new and old experiments, Bretherton [3] further argued that this theoretical estimate of the film thickness is only valid at small capillary numbers.

Following Bretherton's contributions, there has been extensive theoretical and experimental work on the problem of a bubble of either negligible or finite viscosity moving in a tube and displacing a viscous, wetting fluid [4–11]. Experimental results [12], which were later verified by both theory and numerics [13], showed the range of capillary numbers for which Bretherton's theory is valid for an inviscid bubble, and below which the film thickness levels off and becomes independent of the capillary number. Effects of nonwettability were first addressed by [14], who showed numerically that there is a critical capillary number below which steady films of uniform thickness cannot be obtained due to rupture of the film. This result was qualitatively verified by experiments [15]. Other studies of the bubble in a tube problem have accounted for, e.g., flexibility of the substrate, which is an important effect in medical applications such as airway closure [16–22].

In this paper, we are interested in the particular situation of a nonwetting fluid surrounding the bubble, where disjoining pressure in the form of attractive intermolecular forces can be destabilizing (see, e.g., [14] for a review of the various disjoining pressure functions), and consequently, the thin film may rupture. We are motivated by the experimental work of Chen *et al.* [15], who studied the dynamics of oil droplets advancing in a rectangular microchannel filled with water, where one region of the channel was made hydrophobic, while the other was kept hydrophilic. Rupture was observed in the hydrophobic region for slowly moving drops. However, once the drops were advanced at speeds larger than some critical value, it was observed that rupture was suppressed. To this end, we posit a simplified mathematical model to study the transition of a bubble of negligible viscosity from a wetted to a nonwetted region in a circular tube. We solve the model both analytically and numerically, and our results provide conditions under which rupture suppression is attainable. The bubble configuration is illustrated in Fig. 1(a); the subfigures 1(b) and 1(c) show two instances where rupture has occurred near the front or the rear meniscus of the bubble. The surface profiles are plotted from time-dependent numerical simulations of the front and rear menisci. Here, they are shown without scale only so as to illustrate the qualitative phenomena of rupture; see Sec. IV for more details on the numerical implementation.

Note that rupture, or adhesion, is not always a desired phenomenon, especially in applications that involve self-cleaning surfaces [23–25]. However, in some circumstances, rupture can be beneficial, such as in targeted drug delivery [26], or by using the adhesive properties of tumor cells to promote separation from healthy cells [27]. The theoretical approach to thin-film rupture is typically developed in the framework of slow viscous flow (lubrication) theory, by the addition of attractive intermolecular forces, such as van der Waals attractions [28–31]. Self-similar analyses have been provided of rupturing film profiles [32, 33]. Also, studies have been reported of rupture delay by adding surfactants or increasing the flexibility of the substrate supporting the rupturing film [34], and of rupture suppression by adding an external shear to the thin film [35, 36].

We begin this study by developing the theoretical framework in Sec. II for a bubble advancing in a tube, and displacing a nonwetting fluid, where we use lubrication theory to describe the bubble dynamics when attractive van der Waals interactions are substantial. In Sec. III, we study the steady-state profiles of the shape of the bubble as a function of a nondimensional van der Waals

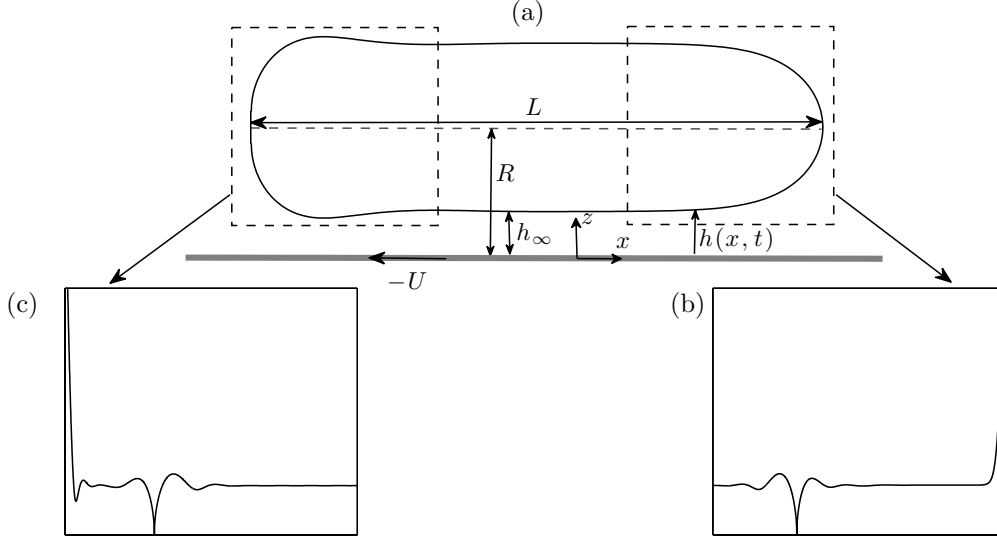


FIG. 1: Bubble translating past a boundary. (a) Bubble interface with two domains highlighted: the front meniscus, and the rear meniscus of the bubble. (b) Rupture of the thin film as a perturbation advances away from the front meniscus. (c) Rupture of the thin film as a perturbation advances towards the rear meniscus.

parameter that characterizes the strength of the intermolecular forces. In Sec. III A, the asymptotic behavior of the steady states is analyzed for small and large values of the van der Waals coefficient, and a relation between film thickness and capillary number is found in Sec. III B. We analyze the unsteady dynamics in Sec. IV; we begin with the case where van der Waals forces are significant throughout the tube and we perform a linear stability analysis as well as a numerical study in Sec. IV A. We then consider the problem of a bubble displacing a wetting fluid, when suddenly attractive van der Waals forces are turned on. The effect on the bubble dynamics is examined as the interface moves from a wetted to a nonwetted region in the tube, and is analyzed both numerically and asymptotically in Sec. IV B. We conclude by finding a critical capillary number beyond which rupture is expected to be suppressed.

II. MATHEMATICAL FORMULATION

Consider a long bubble of negligible viscosity moving at a constant speed U through a capillary tube of radius R , which is filled with a nonwetting fluid of viscosity μ and density ρ . The bubble is assumed to be at least a few tube radii long. The motion of the bubble displaces the viscous fluid, which causes the deposition of a uniform thin film in the annular region between the bubble interface and the tube walls [cf. Fig. 1(a)]. The interfacial tension between the displaced fluid and the bubble is denoted by γ . The deposited film has a thickness h_∞ , and is considered thin enough that intermolecular forces in the form of long range van der Waals attractions are significant, and are measured by the Hamaker constant A , which is typically of the order 10^{-20} to 10^{-19} J.

In the limit that the film thickness is very small compared to the tube radius, the system can be described locally as two-dimensional. Thus, we use Cartesian coordinates (x, z) and time t to describe the spatial and temporal dynamics. The x -coordinate describes lateral positions of the bubble in the tube. We treat the front and rear menisci of the bubble separately, but shall discuss the implications of this assumption in Sec. IV A. When treating the front meniscus of the bubble, we refer to $x \rightarrow \infty$ as the front bubble cap, $x \rightarrow -\infty$ as the uniform thin film of thickness h_∞ . Conversely, when treating the rear meniscus, we refer to $x \rightarrow -\infty$ as the rear bubble cap, $x \rightarrow \infty$

as the uniform thin film of thickness h_∞ .

Following Bretherton [3], we assume that both the Weber number $\rho RU^2/\gamma$ and the Bond number $\rho g R^2/\gamma$ are very small, and we therefore neglect both inertial and gravitational effects. The thickness of the film from the tube wall, $z = 0$, to the bubble interface is denoted by $h(x, t)$, and in the limit that $|\partial_x h| \ll 1$, we can use the lubrication approximation to derive the equation describing thin-film dynamics (cf. Sec. II B in Ref. 37) in the presence of attractive intermolecular forces. The dimensional governing equation, in a frame of reference moving with the advancing bubble, is given by

$$\partial_t h + \frac{1}{3\mu} \partial_x \left[\gamma h^3 \partial_{xxx} h + \frac{A \mathcal{H}(x + Ut)}{2\pi h} \partial_x h \right] - U \partial_x h = 0. \quad (1)$$

Later in Sec. IV B $\mathcal{H}(x + Ut)$ will be chosen to be the Heaviside step function, so that a term proportional to A switches on across $x = -Ut$. This will serve to model a section of the tube that suddenly transitions from wetting to nonwetting.

Throughout the remainder of this section and the next, we assume that $\mathcal{H} \equiv 1$ and hence the intermolecular forces apply throughout the entire length of the tube. Nondimensionalizing (1) yields

$$\partial_T H + \partial_X \left[H^3 \partial_{XXX} H + \frac{\beta}{H} \partial_X H \right] - \partial_X H = 0, \quad (2)$$

where we have set $h = h_\infty H$, $x = (\text{Ca}^{-1/3} h_\infty) X$, $t = (h_\infty \text{Ca}^{-1/3} U^{-1}) T$, and where the capillary number is defined by

$$\text{Ca} = \frac{3\mu U}{\gamma}. \quad (3)$$

In (2), we have also introduced the dimensionless van der Waals parameter,

$$\beta = \frac{A}{2\pi\gamma h_\infty^2 \text{Ca}^{2/3}}. \quad (4)$$

Note that when $\beta < 0$, the intermolecular forces are repulsive, hence stabilizing, and the displaced fluid wets the substrate. When $\beta > 0$, these forces are attractive, thus, the displaced fluid is nonwetting, and rupture may occur. In this work, we are interested in scenarios that may lead to rupture, and hence we consider the situation of a bubble surrounded by a nonwetting fluid in a tube, with $\beta > 0$.

III. STEADY-STATE THEORY ($\mathcal{H} \equiv 1$)

Setting the time derivative in (2) to zero and integrating yields the governing steady-state problem for $H = H_s(X; \beta)$,

$$H_s^3 H_s''' + \beta \frac{H_s'}{H_s} - H_s = -1, \quad (5)$$

with primes (') indicating differentiation in X . The problem has been nondimensionalized so that the steady-state profile approaches a uniform film of unit height in the central region. Thus, for a re-scaled model near the front of the bubble, we require $H_s \rightarrow 1$ as $X \rightarrow -\infty$. For the rear of the bubble, $H_s \rightarrow 1$ as $X \rightarrow \infty$. Setting $H_s = 1 + \eta(X)$, where $|\eta| \ll 1$, we linearize (5) to find the

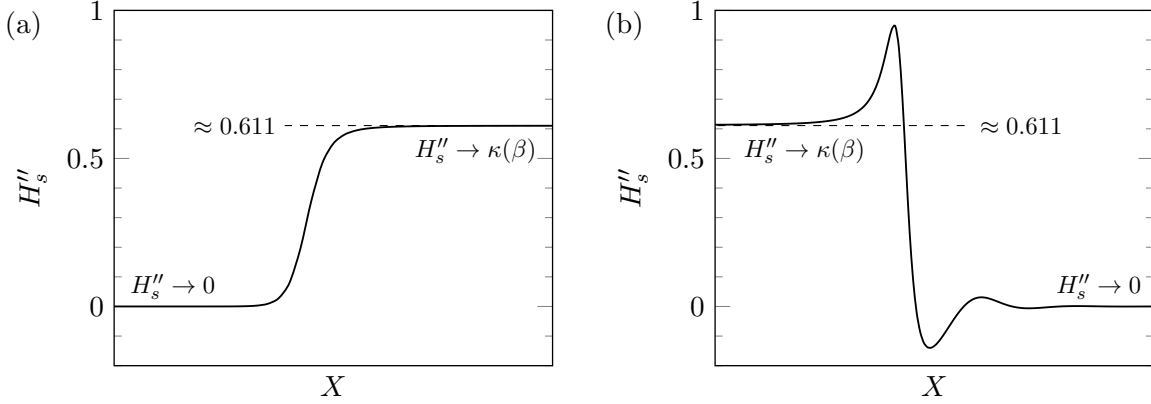


FIG. 2: Variation in linearized curvature of the bubble profile for the (a) front meniscus and (b) rear meniscus. The curvature tends to zero as the film tends towards the central region, and tends to a constant nonzero value $\kappa(\beta)$ towards the front (in a) and rear (in b). For the case of $\beta = 0.2$, we find that $\kappa \approx 0.611$.

perturbation satisfies

$$\eta''' + \beta\eta' - \eta = 0. \quad (6)$$

This equation has solutions of the form $\exp(mX)$, where m is a root of the cubic equation $m^3 + \beta m - 1 = 0$. For $\beta > 0$, this cubic equation has one positive real root, m_1 , and two complex conjugate roots, m_2 and m_2^* .

Solving for the perturbation η , we find the two limiting behaviors that describe the necessary matching conditions between the front or rear of the bubble with the central body. At the front, in order to satisfy the uniform boundary condition when the film tends to the central body, the modes corresponding to the roots m_2 and m_2^* must equal zero. Thus, the solution asymptotes to a uniform film as

$$(\text{for front meniscus}) \quad H_s(X; \beta) \sim 1 + \eta_0 \exp(m_1 X) \quad \text{as } X \rightarrow -\infty, \quad (7)$$

where η_0 is an integration constant, which may be set to unity without loss of generality by exploiting translation invariance. Thus the numerical solution for the front meniscus is found by solving (5) subject to the farfield behavior (7). A typical solution of the curvature H_s'' of the front meniscus is shown in Fig. 2(a). It is observed that the curvature approaches a constant value as $X \rightarrow +\infty$, and we denote this value as $\kappa(\beta) = H_s''(+\infty)$. In the next section, we study the asymptotic behavior of κ as $\beta \rightarrow 0, \infty$.

At the rear meniscus, in order to satisfy the boundary conditions when the film tends to the central body, the eigenfunction of (6) corresponding to m_1 must equal zero. Therefore, the rear meniscus asymptotes to a uniform film as

$$(\text{for rear meniscus}) \quad H_s(X; \beta) \sim 1 + \tilde{\eta}_0 \exp[\text{Re}(m_2)X] \cos[\text{Im}(m_2)X + \phi] \quad \text{as } X \rightarrow +\infty, \quad (8)$$

where the oscillations correspond to capillary ripples at the rear cap of the bubble [3, 38]. Here $\tilde{\eta}_0$ and ϕ are integration constants, and again $\tilde{\eta}_0$ may be set to 1 without loss of generality. Therefore, we use $\phi \in [-\pi, \pi]$ as a shooting parameter, and find the value ϕ^* of ϕ such that the curvature of the rear meniscus of the bubble is equal to that of the front, $\kappa(\beta)$. For example, for the case $\beta = 0.2$, this parameter is found to be $\phi^* \approx -1.4$. In Fig. 2(b) we show the curvature H_s'' of the rear meniscus for a given β . The behavior of the curvature as a function of β is summarized in Fig. 3.

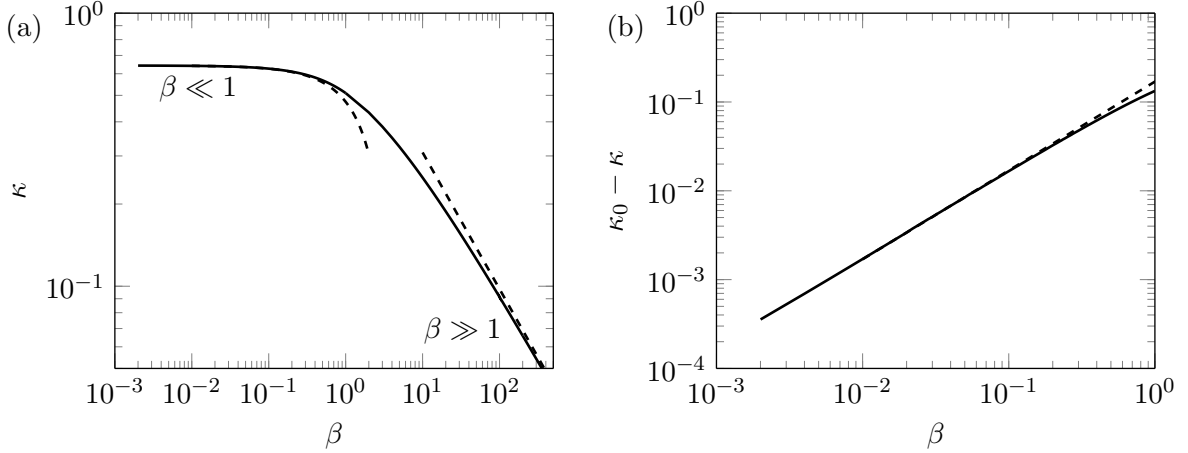


FIG. 3: (a) Curvature of the front meniscus as a function of the van der Waals parameter β . Numerical results are shown solid, and asymptotic approximations, from (11) and (17), are shown dashed. In (b) a zoom of the region of small β shows $\kappa_0 - \kappa \sim \kappa_1 \beta$ as $\beta \rightarrow 0$.

Since $H_s'' \sim \kappa(\beta)$, we can redimensionalize to see that κ is related to the uniform film thickness h_∞ in the bubble by

$$\frac{h_\infty}{R} = \kappa(\beta) \text{Ca}^{2/3}. \quad (9)$$

The relation in (9) provides an implicit description of how the film thickness varies as a function of the van der Waals coefficient β for any $\beta > 0$.

A. Asymptotic Behavior of $\kappa(\beta)$

When $\beta = 0$, Bretherton [3] had shown that $h_\infty/R \sim \kappa_0 \text{Ca}^{2/3}$ where $\kappa_0 \approx 0.643$. However, when $\beta > 0$, we observe from (9) that the variation of the meniscus curvature, κ , must lead to a modification of Bretherton's result. In what follows, we elucidate this effect by determining κ in the limits of large and small β . Note that in our steady-state model, we have assumed that the front meniscus sets the curvature which is then imposed on the rear; hence it is only necessary to perform our analysis on the front of the bubble.

In the limit of $\beta \rightarrow 0$, we expand $H_s = H_0 + \beta H_1 + O(\beta^2)$. Substituting the perturbation expansion into the governing equation (5), yields for the first two orders,

$$H_0''' = (H_0 - 1)H_0^{-3}, \quad (10a)$$

$$H_1''' + (2H_0^{-3} - 3H_0^{-4})H_1 = -H_0' H_0^{-4}, \quad (10b)$$

subject to the boundary condition (7), or that $H_0 \sim 1 + \eta_0 \exp(X)$ and $H_1 \rightarrow 0$ in the limit $X \rightarrow -\infty$. The leading-order equation in (10a) is Bretherton's original equation (also known as the Landau-Levich equation). Numerical solutions of H_0 and H_1 confirm that the curvature at the front, measured from the second derivative of H_s , is given by a series expansion in powers of β , or

$$\kappa(\beta) \sim \kappa_0 + \kappa_1 \beta + \dots \quad \text{as } \beta \rightarrow 0, \quad (11)$$

where $\kappa_0 \approx 0.643$ and $\kappa_1 \approx -0.169$. Thus, when $\beta = 0$ we recover Bretherton's result, with $\kappa = \kappa_0$.

In order to observe the dependence of κ at larger values of β , consider the limit $\beta \rightarrow \infty$. To reincorporate the spatial variation in this limit, we introduce the stretched coordinate $\tilde{X} = X/\beta$, with $H_s = G(\tilde{X})$. The governing equation (5) then becomes

$$\frac{1}{\beta^3} G^3 G''' + \frac{G'}{G} + 1 - G = 0, \quad (12)$$

with primes now denoting derivatives with respect to \tilde{X} . Neglecting the first term of (12) yields the leading-order result,

$$G \sim \left[1 - \exp(\tilde{X} - \tilde{X}_0)\right]^{-1}, \quad (13)$$

where the integration constant \tilde{X}_0 corresponds to an arbitrary translation in \tilde{X} . We shall refer to (13) as the outer solution, which automatically satisfies the farfield condition $G \rightarrow 1$ as $\tilde{X} \rightarrow -\infty$. The asymptotic solution (13) predicts blowup of the film thickness as $\tilde{X} \rightarrow \tilde{X}_0$, and so we shall seek a boundary layer near the transition point $\tilde{X} = \tilde{X}_0$ where the dominant balance in (12) incorporates the surface tension term.

We refer to the solution near $\tilde{X} = \tilde{X}_0$, as the inner solution. From a dominant balance of (12) and (13), it is found that the correct re-scaling is $\tilde{X} = \tilde{X}_0 + \beta^{-1/2} \hat{X}$ and $G(\tilde{X}) = \beta^{1/2} g(\hat{X})$. This transforms (12) into

$$g^3 g''' + \frac{g'}{g} - g = -\frac{1}{\sqrt{\beta}}, \quad (14)$$

with primes now denoting differentiation with respect to \hat{X} . As $\beta \rightarrow \infty$, the inner solution is expressed as an asymptotic expansion of the form $g \sim g_0 + \beta^{-1/2} g_1 + O(\beta^{-1})$. The leading- and first-order solutions satisfy the differential equations

$$g_0^3 g_0''' + \frac{g_0'}{g_0} - g_0 = 0, \quad (15a)$$

$$g_0^3 g_1''' + \frac{g_1'}{g_0} + \left[2 - 4g_0' g_0^{-2}\right] g_1 = -1. \quad (15b)$$

In order to match the inner solutions with (13) as $\hat{X} \rightarrow -\infty$, g_0 and g_1 are expanded in inverse powers of \hat{X} . Substitution into (15) then yields the far-field conditions

$$g_0 = -\frac{1}{\hat{X}} + \frac{6}{5\hat{X}^7} + \dots, \quad g_1 = \frac{1}{2} - \frac{3}{\hat{X}^6} + \dots, \quad \text{as } \hat{X} \rightarrow -\infty. \quad (16)$$

The inner solutions g_0 and g_1 are numerically computed by solving (15) as an initial-value problem subject to (16) applied at large negative \hat{X} . The differential equations (15) are then integrated to a large positive value of \hat{X} such that the curvatures g_0'' and g_1'' reach constant values $\kappa_{\text{in}0}$ and $\kappa_{\text{in}1}$, respectively. Hence, the large- β asymptotic behavior of the function κ is found to be

$$\kappa = \frac{\kappa_{\text{in}0}}{\beta^{1/2}} + \frac{\kappa_{\text{in}1}}{\beta} + \dots \quad \text{as } \beta \rightarrow \infty, \quad (17)$$

where $\kappa_{\text{in}0} \approx 0.977$ and $\kappa_{\text{in}1} \approx -0.657$. The asymptotic results (11) and (17) are displayed as dashed lines in Fig. 3, and are in excellent agreement with the numerical solution of the steady-state differential equation (5).

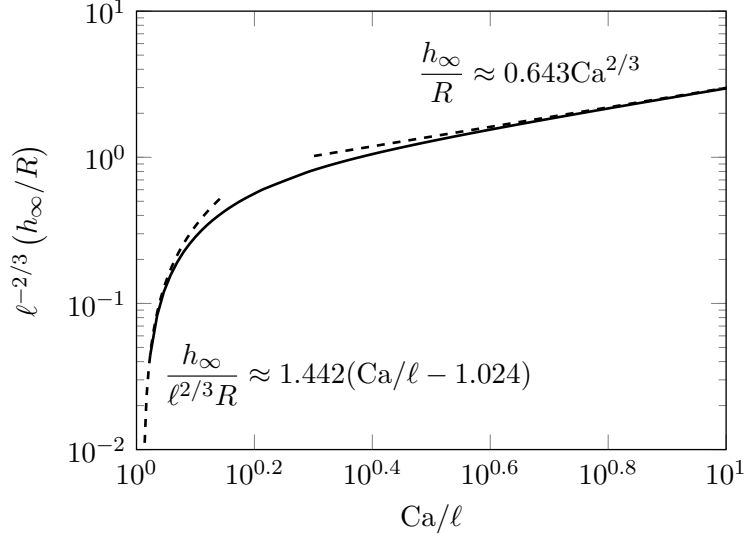


FIG. 4: The relation between the normalized film thickness $\ell^{-2/3}h_\infty/R$ and the scaled capillary number $\ell^{-1}\text{Ca}$, given parametrically by (19). The dashed curves show the two respective asymptotic limits (20a) as $\beta \rightarrow 0$ and (21) as $\beta \rightarrow \infty$.

B. A modification of the Bretherton relation

In Bretherton's work [3], corresponding to $\beta = 0$, the normalized film thickness h_∞/R scales with $\text{Ca}^{2/3}$. Our generalized relation (9) depends implicitly on both h_∞/R and Ca through the van der Waals parameter β , defined by (4). To unravel the dependence of the deposited film thickness on the capillary number, it is helpful to define an additional dimensionless parameter

$$\ell = \left(\frac{A}{2\pi\gamma R^2} \right)^{1/2}, \quad (18)$$

which corresponds to a molecular length scale that depends only on the physical properties of the fluid and the tube radius R . Typical values of the Hamaker constant A are in the range 10^{-20} to 10^{-19} J, the interfacial tension γ has an order of magnitude of about 10^{-2} J/m², and R may be from a few to a few hundred microns. Therefore, ℓ is typically small, taking values in the range of 10^{-6} to 10^{-3} .

We use (4) and (9) to express both h_∞/R and Ca as functions of ℓ and β , namely,

$$\ell^{-1}\text{Ca} = \frac{1}{\beta^{1/2}\kappa(\beta)} \quad \text{and} \quad \ell^{-2/3} \left(\frac{h_\infty}{R} \right) = \left(\frac{\kappa(\beta)}{\beta} \right)^{1/3}. \quad (19)$$

As β ranges between 0 and ∞ , (19) parametrically defines a functional relationship between $\ell^{-2/3}h_\infty/R$ and $\ell^{-1}\text{Ca}$, which is plotted as a solid curve in Fig. 4. This indicates that the film thickness h_∞ is an increasing function of the capillary number, as expected. The detailed behavior may be clarified by using the asymptotic approximations of $\kappa(\beta)$ obtained above. We point out that the bubble must always fit in the tube, and therefore the apparently unbounded increase of the film thickness with capillary number must be regularized for large values of Ca [39, 40]. This, however, is not analyzed in the current study.

Considering the small and large limits of β , and combining (11) and (17) with (19), we obtain

$$\ell^{-1}\text{Ca} \sim \frac{1}{\kappa_0}\beta^{-1/2}, \quad \ell^{-2/3}\frac{h_\infty}{R} \sim \kappa_0^{1/3}\beta^{-1/3} \sim \kappa_0 \left(\frac{\text{Ca}}{\ell}\right)^{2/3} \quad \text{for } \beta \rightarrow 0, \quad (20a)$$

$$\ell^{-1}\text{Ca} \sim \frac{1}{\kappa_{\text{in}0}} + \frac{|\kappa_{\text{in}1}|}{\kappa_{\text{in}0}^2}\beta^{-1/2}, \quad \ell^{-2/3}\frac{h_\infty}{R} \sim \kappa_{\text{in}0}^{1/3}\beta^{-1/2} \quad \text{for } \beta \rightarrow \infty, \quad (20b)$$

where $\kappa_0 \approx 0.643$, $\kappa_{\text{in}0} \approx 0.977$, and $\kappa_{\text{in}1} \approx -0.657$. The latter equation (20b) can be rearranged to

$$\frac{h_\infty}{\ell^{2/3}R} \sim \frac{\kappa_{\text{in}0}^{7/3}}{|\kappa_{\text{in}1}|} \left(\frac{\text{Ca}}{\ell} - \frac{1}{\kappa_{\text{in}0}} \right) \approx 1.442 \left(\frac{\text{Ca}}{\ell} - 1.024 \right) \quad \text{for } \beta \rightarrow \infty. \quad (21)$$

The dashed curves in Fig. 4 verify that the approximate relations (20a) and (21) are approached in the relevant limits.

We can interpret the results as follows: first, Bretherton's result is recovered when β is small, which corresponds to the capillary number being sufficiently large, namely,

$$\ell \ll \text{Ca} \ll 1. \quad (22)$$

Second, the relation between h_∞/R and Ca starts to depart significantly from Bretherton's prediction when $\text{Ca} = O(\ell)$. From (21), it is expected that in the limit $\beta \rightarrow \infty$, the film thickness, h_∞ , left behind the front meniscus reaches zero at a finite critical value of the capillary number,

$$\text{Ca}^* \approx 1.024\ell. \quad (23)$$

As noted above, ℓ typically ranges between 10^{-6} and 10^{-3} . Thus, for capillary numbers smaller than this value, no steady film will be left behind the advancing front meniscus. This result differs quite significantly from the case where the surrounding fluid wets the substrate ($\beta \leq 0$). In that case, the departure from Bretherton's results for $\text{Ca} = O(\ell)$ is characterized by a uniform film independent of capillary number [12, 13].

IV. UNSTEADY SOLUTIONS

So far, we have shown that for a bubble moving in a tube and subject to attractive van der Waals forces, steady-state free-surface profiles may exist for $\beta > 0$. For β sufficiently small, the central film thickness will follow relation (9). For β sufficiently large, however, steady-state profiles with a constant-height central region may not exist for sufficiently small Capillary numbers; this threshold is difficult to specify precisely [cf. (9)] due to the fact that it likely involves the global flow characteristics of the bubble and channel. Thus in the following numerical analysis, we shall focus moreso on the physically relevant (and tractable) regime of small-to-moderate β .

The next question is whether such steady-state solutions remain stable or become unstable once they are evolved in time. Our efforts in this section are divided into two parts. In Sec. IV A the stability of the bubble is studied using numerical simulations of the central thin-film and meniscus regions, where van der Waals forces are assumed to be substantial throughout the entire length of the tube. Here we shall confirm the dependence of the rupture time T_r on β . Then, in Sec. IV B we shall propose a model where the bubble moves from a wetted region ($\beta = 0$) to a nonwetted region ($\beta > 0$) in the tube. Here we show that the rupture time differs from that obtained in the case where van der Waals forces are significant everywhere in the tube.

A. Evolution of a bubble subject to van der Waals attractions everywhere ($\mathcal{H} \equiv 1$)

Let us consider the linear stability of the time-dependent equation (2) about a base state that consists of a uniform film. Perturbing the film, we set $H = 1 + \epsilon \exp(ikX + \omega T)$ and linearize for infinitesimal perturbations in the limit $\epsilon \ll 1$. This yields the dispersion relation

$$\omega = -k^4 + \beta k^2 + ik, \quad (24)$$

between the linear growth rate ω and the wave number k . The result is essentially the same as the dispersion relation obtained for a stationary film subject to viscous, surface tension, and van der Waals forces [36] except for the addition of a traveling wave term ik . Thus, according to (24), linear theory predicts that the film is stable for $\beta \leq 0$ and unstable to long-wave perturbations for any $\beta > 0$. Moreover from (24), we find that the most rapidly growing mode, i.e., the wavenumber k_c that maximizes $\text{Re}(\omega)$, corresponds to respective wavelengths and growth rates of

$$\lambda_c = 2\pi/k_c = 2\pi\sqrt{2/\beta} \quad \text{and} \quad \text{Re}(\omega_c) = -k_c^4 + \beta k_c^2 = \beta^2/4. \quad (25)$$

We conclude that wavelengths of order $\beta^{-1/2}$ or longer are expected to be unstable, and that the characteristic time for the instability to occur should be proportional to β^{-2} . In order to verify this basic stability calculation, and to demonstrate how the rupture-time can be controlled by adjustments to the van der Waals parameter, we design the following simplified numerical experiment.

A bubble displaces a nonwetting fluid that is present throughout a tube. The evolution of the bubble is thus described by (2), or equivalently (1) with $\mathcal{H} \equiv 1$. We impose that it begins from

$$H = H_s(X; \beta) \quad \text{at } T = 0, \quad (26)$$

where $H_s(X; \beta)$ describes the shape of either the front or rear meniscus at steady state [cf. Sec. III]. In order to avoid modeling the entire topology of the bubble, we assume that, through its evolution, the film profile remains quasi-static near the front or rear. In the case of modeling the front of the bubble, we impose that

$$H \rightarrow 1 \quad \text{and} \quad \partial_X H \rightarrow 0 \quad \text{as } X \rightarrow -\infty \text{ (towards central region)}, \quad (27a)$$

$$H \sim H_s(X; \beta) \quad \text{as } X \rightarrow +\infty \text{ (towards meniscus)}. \quad (27b)$$

To model the rear, the limits in X are swapped. Condition (27b) requires that the curvature of the profile, $\partial_{XX} H$, match with $H_s'' \sim \kappa(\beta)$, which corresponds to the linearized curvature of the meniscus. Our model assumes that the front and rear menisci are static during the instability regime and do not interact with one another. Thus, the evolution primarily occurs in the central region of the bubble. We return to discuss the possibility of numerical simulations of the full bubble topology in Sec. V.

To solve the time-dependent formulation, an implicit-explicit numerical scheme is used, which computes nonlinear terms of H in (2) explicitly, while the linear terms of H and its derivatives are treated implicitly for increased stability. Centered differences are employed in both the spatial and temporal coordinates. We use a uniform spatial grid with step size ΔX (typically between 10^{-2} and 10^{-3}), and an adaptive time step that decreases with the growth of the maximum traveling-wave amplitude (typically between 10^{-3} and 10^{-8}). Further details of this numerical scheme are presented in Appendix B in [41] or Appendix A in [42].

When the initial condition (26) is evolved in time, a perturbation appears near the front meniscus and grows in amplitude as it travels towards the central body of the bubble. If the amplitude grows

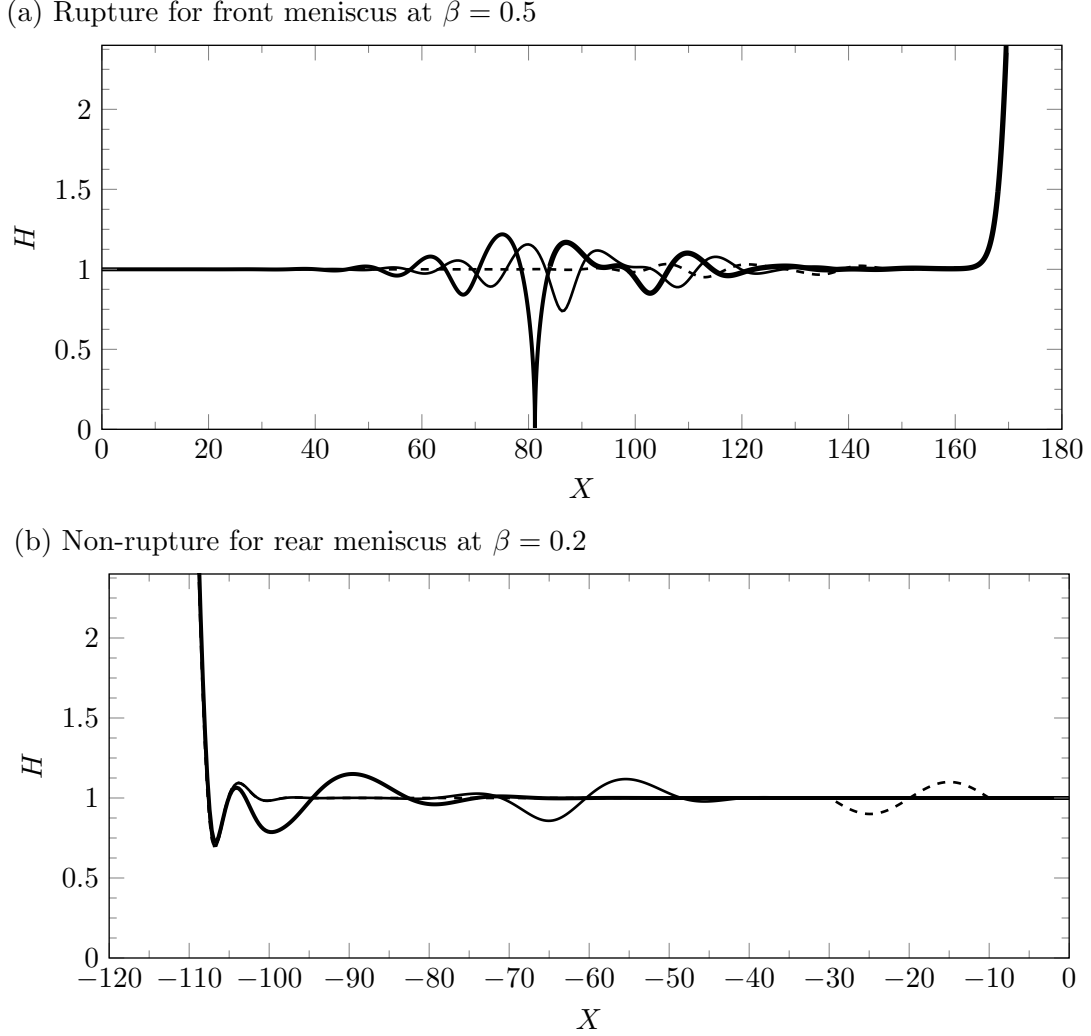


FIG. 5: (a) Evolution to rupture for the case of the central film near the front meniscus, with $\beta = 0.5$ at $T = 56.95$ (dashed), 83.65 (solid), 88.84 (thick). (b) Evolution of the rear meniscus with $\beta = 0.2$ at $T = 0$ (dashed), $T = 40.3$ (solid), $T = 74.4$ (thick). The initial profile is perturbed with an additional localized sinusoidal perturbation. The film does not rupture; at large time, it is indistinguishable to graphical accuracy from the unperturbed initial state.

sufficiently, rupture occurs. Fig. 5a shows a typical result corresponding to evolution near the front meniscus for the case $\beta = 0.5$. Simulations are run for different values of β (typically ranging from 0.1 to 1). For each run, we observe the time it takes for rupture to occur, T_r .

Note that the initial perturbation leading to growth in Fig. 5a is due to a mismatch between the exact steady-state profile (applied to a semi-infinite domain and with a gradient tending to infinity at the front meniscus) and our numerical approximation of H_s applied on a truncated domain. Other perturbations can be used. For example, we may begin from the steady-state, plus a small localized sinusoidal perturbation added to the central region. In Fig. 5b, the rear of the bubble is modeled at $\beta = 0.2$. Here the initial condition is shown dashed, and includes the sinusoidal perturbation. The perturbed region is shown to grow and advect towards the rear of the bubble, where it is absorbed into the meniscus. As time is further increased, the film settles to its numerically exact steady state. Thus, in the case of the rear meniscus, for sufficiently small perturbations or sufficiently small β , rupture is suppressed. For the front meniscus, rupture always

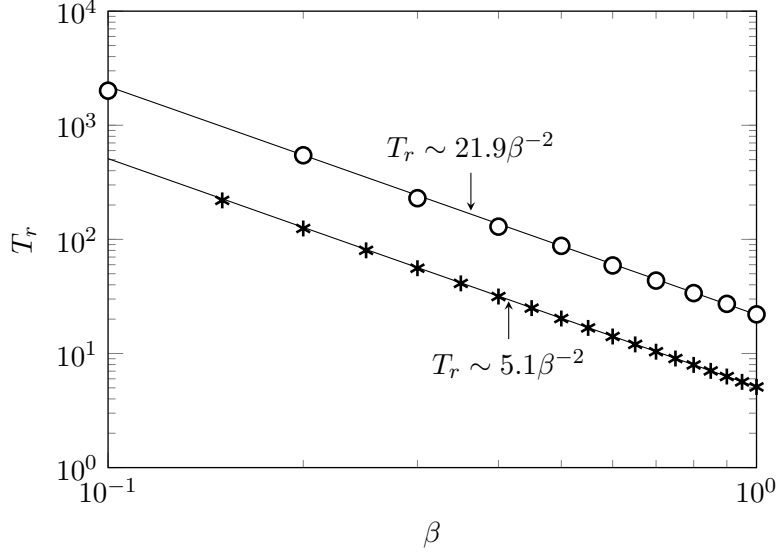


FIG. 6: Rupture time T_r plotted against β . Within the range of β shown, the rupture time is proportional to β^{-2} . The slower trend (stars) corresponds to beginning at the approximated steady-state; the faster trend (circles) corresponds to beginning from the steady-state plus a localized sinusoidal perturbation.

occurs as long as the computational domain of the central body is sufficiently long.

The graph of rupture time T_r as a function of β is shown in Fig. 6 for two initial conditions of the front meniscus. Here it is confirmed that $T_r \sim \alpha/\beta^2$ as predicted from the linear stability analysis. Different small perturbations affect the pre-factor α of the rupture trend but not the power-law. In the figure, the slower rupture trend ($T_r \approx 5.1\beta^{-2}$) corresponds to beginning at the approximated steady-state; the faster trend ($T_r \approx 21.9\beta^{-2}$) corresponds to beginning from the steady-state plus a localized sinusoidal perturbation (see Fig. 5b for example of such a perturbation). The points in the figure are confirmed to converge as the domain size is extended, or if finer spatial and temporal discretizations are used.

Based on these numerical results, we summarize as follows: given a value $0 < \beta \ll 1$, a traveling wave perturbation moves from the front meniscus towards the rear and grows until either (i) rupture occurs in the central region of the bubble; or (ii) the wave reaches the rear meniscus, where the van der Waals forces are minimal, and rupture is suppressed.

The numerical simulations of this section only provide a simplified model of the full bubble dynamics on account of two limiting assumptions. First, the bubble is assumed to begin from a pre-existing quasi-steady state. Second, the bubble's global configuration within the channel is largely ignored. However, given that the time-scale for rupture is $O(1/\beta^2)$ in the limit of small perturbations, it can be verified from the dispersion relation of (24) that a localized disturbance is expected to rupture a distance $O(1/\beta^2)$ from its initial conception. Thus, based on this simplified model, it can be expected that bubbles with a non-dimensional length $\ll O(1/\beta^2)$ will remain stable.

B. Evolution of a bubble subject to van der Waals forces in one section of the tube

As noted in Sec. IV A above, when van der Waals forces are significant throughout the entire length of the tube, the time it takes for a quasi-static bubble to rupture is proportional to β^{-2} . Now we consider a situation where the destabilizing disjoining pressure is only present in one section of a

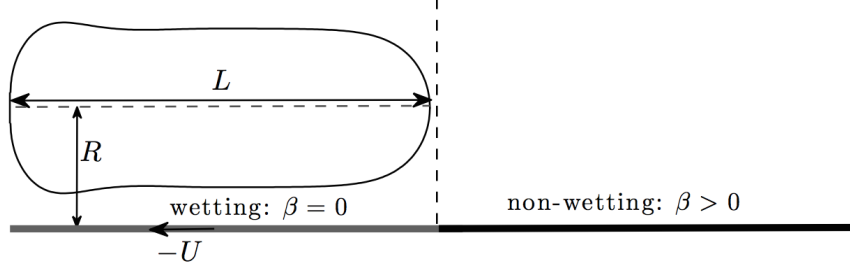


FIG. 7: Schematic showing the section of a tube where the disjoining pressure is switched on. The bubble translates across a section of the surface where the wetting state changes (from wetting to non-wetting). This is modeled as a step transition in the thin-film equation (1).

tube (Fig. 7). We find how the rupture time varies as a function of the van der Waals coefficient β and hence estimate the critical capillary number above which rupture is expected to be suppressed. We thus use the dimensional governing equation (1) and choose \mathcal{H} to be the Heaviside step function so that the term proportional to A switches on across $x = -Ut$.

Note that when t is negative and before the front meniscus has reached $x = -Ut$, there is no disjoining pressure effect and the problem reduces to Bretherton's model [3]. In this case, the film thickness is given by (9) with $\kappa = \kappa_0 \approx 0.643$, and we now use this thickness specifically when nondimensionalizing (1). The definition (4) of β is replaced by a new dimensionless parameter

$$\tilde{\beta} = \frac{A}{2\pi\gamma R^2 \kappa_0^2 \text{Ca}^2} = \frac{\ell^2}{\kappa_0^2 \text{Ca}^2}, \quad (28)$$

where ℓ is defined by equation (18), and we introduce new dimensionless variables:

$$h(x, t) = \left(\kappa_0 R \text{Ca}^{2/3}\right) \eta(\xi, \mathcal{T}), \quad x = \left(\kappa_0 R \text{Ca}^{1/3}\right) \xi, \quad t = \left(\kappa_0 R \text{Ca}^{1/3} U^{-1}\right) \mathcal{T}. \quad (29)$$

Then, from (1) the governing system for the front meniscus becomes

$$\partial_{\mathcal{T}} \eta + \partial_{\xi} \left[\eta^3 \partial_{\xi\xi\xi} \eta + \tilde{\beta} \frac{\mathcal{H}(\mathcal{T} + \xi)}{\eta} \partial_{\xi} \eta - \eta \right] = 0. \quad (30a)$$

$$\eta \rightarrow 1 \quad \text{as } \xi \rightarrow -\infty, \quad \partial_{\xi\xi} \eta \rightarrow \kappa_0 \quad \text{as } \xi \rightarrow +\infty, \quad (30b)$$

$$\eta \rightarrow H_s(\xi; 0) \quad \text{as } \mathcal{T} \rightarrow -\infty. \quad (30c)$$

We are interested in solutions of the problem (30) in the physically relevant regime where $\tilde{\beta} \ll 1$. When \mathcal{T} is large and negative, η approaches $H_s(\xi; \beta = 0)$, which is the steady solution to Bretherton's problem introduced in Sec. III. On the other hand, when $\mathcal{T} \gg 1$, we expect the solution near the front meniscus to become quasi-steady again, but now with a thinner deposited film due to the attractive intermolecular forces. The asymptotic analysis of Sec. III A implies that the resulting decrease in the deposited film thickness is small when $\tilde{\beta} \ll 1$, so that the value of η left behind the front meniscus decreases from 1 to approximately $1 - \nu$, where the small parameter ν is defined by

$$\nu = \frac{|\kappa_1|}{\kappa_0} \tilde{\beta} = \frac{|\kappa_1|}{\kappa_0^3} \frac{\ell^2}{\text{Ca}^2} \approx 0.636 \frac{\ell^2}{\text{Ca}^2} \ll 1. \quad (31)$$

We deduce that the situation for $\mathcal{T} > 0$ is as depicted schematically in Fig. 8. The deposited

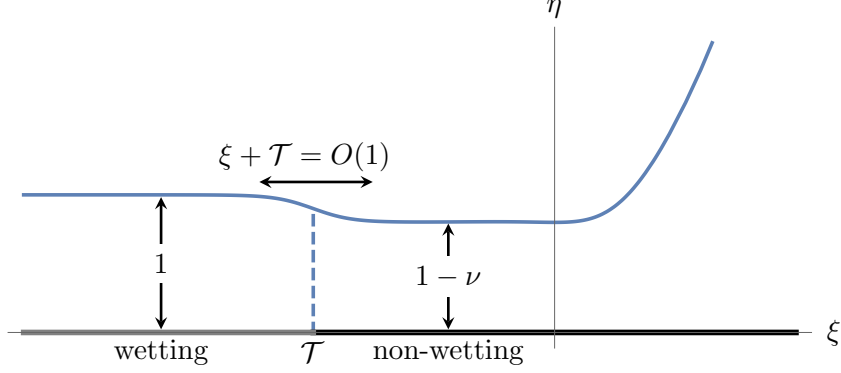


FIG. 8: Schematic of the film deposited behind the front meniscus as it crosses from the wetting to the non-wetting section of the tube.

film thickness transitions from 1 to $1 - \nu$ in an $O(1)$ neighborhood of the point $\xi = -\mathcal{T}$ where the tube wall switches from wetting to non-wetting. In the subsequent evolution, we expect the deposited film to lose stability, due to the attractive van der Waals forces, and ultimately rupture. However, the linear stability analysis of Sec. IV A informs us that, in the physically relevant regime where $\tilde{\beta}$ is small, the dominant length- and time-scales for the instability are both much larger than those used in the nondimensionalization (29).

To follow the progress of the instability, we therefore shift to a frame that follows the transition point $\xi = -\mathcal{T}$ while re-scaling to reflect the relevant length- and time-scales as follows:

$$\xi + \mathcal{T} = \tilde{\beta}^{-1/2}\zeta \quad \text{and} \quad \mathcal{T} = \tilde{\beta}^{-2}\tau. \quad (32)$$

Equation (30a) is thus transformed to

$$\partial_\tau \eta + \partial_\zeta \left[\eta^3 \partial_{\zeta\zeta\zeta} \eta + \frac{\mathcal{H}(\zeta)}{\eta} \partial_\zeta \eta \right] = 0. \quad (33a)$$

Initial and boundary conditions are found by matching with the large- \mathcal{T} solution of (30a), as sketched in Fig. 8. Following the rescaling (32), the transition between the deposited thicknesses $\eta = 1$ and $\eta = 1 - \nu$ occurs in a vanishingly small neighborhood of $\zeta = 0$ in the limit as $\tilde{\beta} \rightarrow 0$. Therefore the initial film profile appears effectively discontinuous across $\zeta = 0$, and we therefore impose the boundary and initial conditions

$$\eta \rightarrow 1 \quad \text{as } \zeta \rightarrow -\infty, \quad (33b)$$

$$\eta \rightarrow 1 - \nu \quad \text{as } \zeta \rightarrow +\infty, \quad (33c)$$

$$\eta = 1 - \nu \mathcal{H}(\zeta) \quad \text{at } \tau = 0. \quad (33d)$$

1. Numerical solution in the traveling frame

For each given value of ν , we solve the problem (33) numerically using the method of lines (see, e.g., [43]). A sample solution is shown in Fig. 9(a), with $\nu = 0.1$. The discontinuous initial condition is instantaneously smoothed out, as illustrated in Fig. 9(b), and it can be verified that

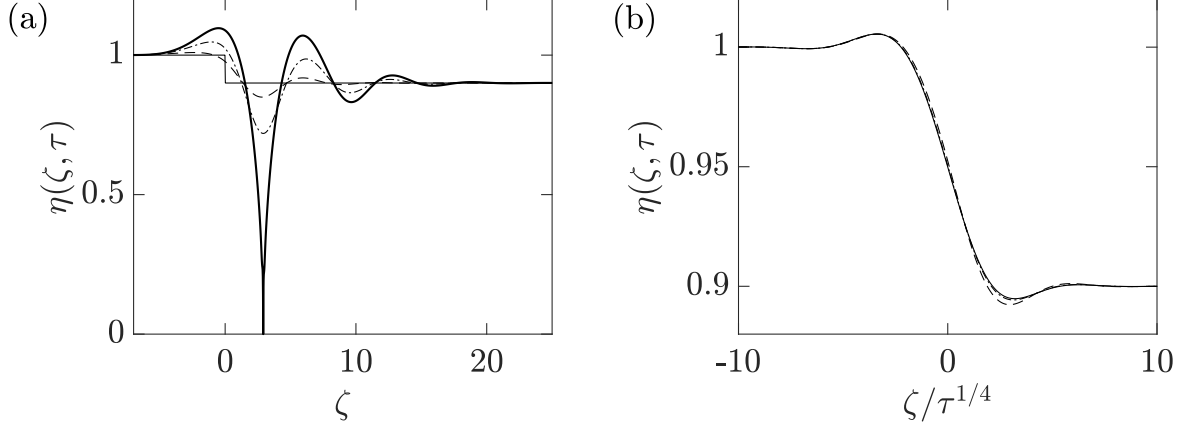


FIG. 9: (a) The numerical solution $\eta(\zeta, \tau)$ of the problem (33) with $\nu = 0.1$ and $\tau = 0, 3, 6, 7.2404$. (b) The solution plotted versus the similarity variable $\zeta/\tau^{1/4}$ for $\tau = 0.001, 0.01, 0.1$; the dashed curve shows the similarity solution (34).

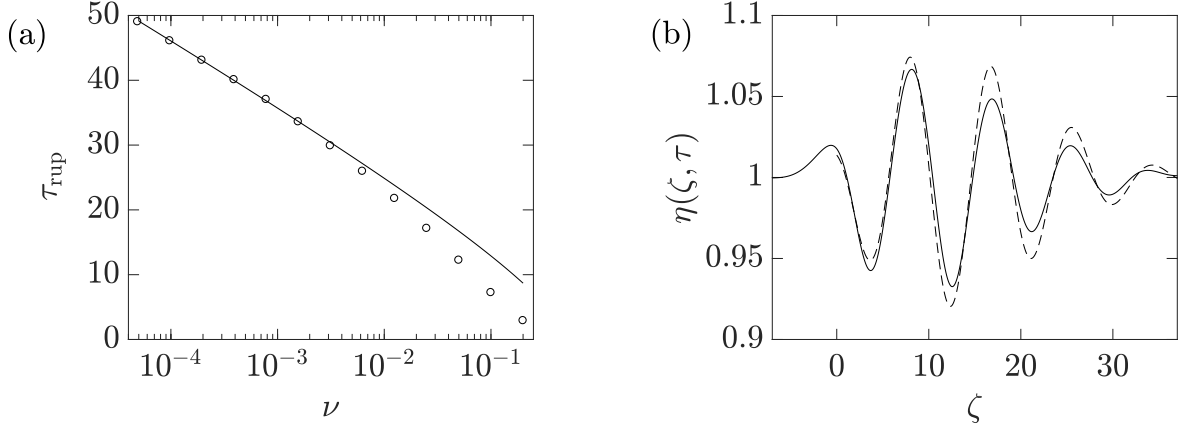


FIG. 10: (a) Log-linear plot of the normalized rupture time τ_{rup} versus the scaled van der Waals parameter ν . The circles show the results obtained from numerical solutions of (33); the solid curve shows the asymptotic prediction (38) with $C = 0.3$. (b) Numerical solution of (33) with $\nu = 0.0001$ and $\tau = 40$; the dashed curve shows the large- τ asymptotic solution $1 - \nu\eta_1$, with η_1 given by Eq. (36).

$\eta(\zeta, \tau)$ approaches the similarity solution

$$\eta(\zeta, \tau) \sim 1 - \nu f\left(\zeta/\tau^{1/4}\right) \quad \text{as } \tau \rightarrow 0, \quad (34a)$$

$$f(z) = \frac{1}{2} + \frac{\Gamma(5/4)z}{\pi} {}_1F_3\left(\frac{1}{4}; \frac{1}{2}, \frac{3}{4}, \frac{5}{4}; \frac{z^4}{256}\right) + \frac{\Gamma(-1/4)z^3}{96\pi} {}_1F_3\left(\frac{3}{4}; \frac{5}{4}, \frac{3}{2}, \frac{7}{4}; \frac{z^4}{256}\right), \quad (34b)$$

where Γ and ${}_1F_3$ denote, respectively, the gamma function and the generalized hypergeometric function. This solution corresponds to related problems of capillary leveling of a thin film [44]; an analogous similarity solution arises in studies of the deformation of an elastica in a viscous fluid [45]. In Fig. 9(a), as τ increases, the instability starts to take effect in $\zeta > 0$, where the disjoining pressure term is present. We observe wave-like disturbances that grow in amplitude, culminating in rupture of the film after a finite time $\tau_{\text{rup}} \approx 7.24$, computed numerically. This rupture time can be determined analytically in the limit of $\nu \rightarrow 0$, and we perform this calculation next.

2. Asymptotic Rupture Time

As shown by the numerical results in Fig. 10(a), the rupture time τ_{rup} increases as the value of ν decreases. To examine the limiting behavior as $\nu \rightarrow 0$, we set $\eta = 1 - \nu\eta_1 + O(\nu^2)$ into (33), and we find that η_1 satisfies the linear PDE

$$\partial_\tau \eta_1 + \partial_{\zeta\zeta\zeta} \eta_1 + \partial_\zeta [\mathcal{H}(\zeta) \partial_\zeta \eta_1] = 0, \quad (35a)$$

along with the boundary and initial conditions

$$\eta_1 \rightarrow 0 \text{ as } \zeta \rightarrow -\infty, \quad \eta_1 \rightarrow 1 \text{ as } \zeta \rightarrow +\infty, \quad \eta_1 = \mathcal{H}(\zeta) \text{ at } \tau = 0. \quad (35b)$$

The solution $\eta_1(\zeta, \tau)$ can be found by taking a Laplace transform in τ . The resulting inversion integral is unwieldy but may be analyzed in the limit of large τ by using the method of steepest descents. A lengthy calculation (given in Appendix A in Ref. 41) leads to the following asymptotic approximation for the solution when $\zeta > 0$ and $\tau \gg 1$:

$$\eta_1(\zeta, \tau) \sim 1 + \frac{1}{\sqrt{\pi} \tau^{3/2}} \exp\left(\frac{\tau}{4} - \frac{\zeta^2}{8\tau}\right) \left[(4 + \zeta) \sin\left(\frac{\zeta}{\sqrt{2}}\right) - \sqrt{2}(2 + \zeta) \cos\left(\frac{\zeta}{\sqrt{2}}\right) \right]. \quad (36)$$

In Fig. 10(b) we illustrate the accuracy of this approximation by plotting the numerical solution of (33) for $\eta(\zeta, \tau)$ with $\nu = 0.0001$ and $\tau = 40$ (solid curve) along with the approximation (36).

Equation (36) implies that the maximum value of η_1 occurs when $\zeta \sim 2\tau^{-1/2}$ and is given approximately by

$$\eta_{1\text{max}}(\tau) \sim 2\sqrt{\frac{3}{\pi e}} \frac{e^{\tau/4}}{\tau} \text{ as } \tau \rightarrow \infty. \quad (37)$$

When τ is so large that the perturbation η_1 becomes of order $1/\nu$, the asymptotic ansatz $\eta \sim 1 - \nu\eta_1$ ceases to be valid, and one must resort to numerical solution of the full governing equation (33a). However, we can anticipate that the subsequent nonlinear evolution and rupture take place over an $O(1)$ time-scale. We can therefore invert (37) to obtain an estimate for the normalized time τ_{rup} taken for the film to rupture, namely,

$$\tau_{\text{rup}} \sim 4 \log(1/\nu) + 4 \log \log(1/\nu) + C, \quad (38)$$

where C is an $O(1)$ constant. The solid curve in Fig. 10(a) demonstrates that (38) provides a very good fit for the behavior of τ_{rup} as $\nu \rightarrow 0$, with $C \approx 0.3$.

3. Prediction of the Critical Capillary Number

By reversing the nondimensionalization (29), we infer from (38) the corresponding dimensional rupture time, namely,

$$t_{\text{rup}} = \frac{\kappa_0 R \text{Ca}^{1/3}}{\tilde{\beta}^2 U} \tau_{\text{rup}} = \frac{\kappa_0^5 R \text{Ca}^{13/3}}{\ell^4 U} \tau_{\text{rup}}. \quad (39)$$

As discussed in Sec. IV A, if t_{rup} is greater than the transit time over the length of the bubble, L/U , then the free-surface disturbance will be swept up by the rear meniscus before rupture has time to occur. Thus, by setting $t_{\text{rup}} = L/U$ we can find the value of the critical capillary number Ca_{crit}

above which rupture is expected to be suppressed, i.e.,

$$\frac{L}{R} = \frac{\kappa_0^5 \text{Ca}_{\text{crit}}^{13/3}}{\ell^4} \tau_{\text{rup}} \approx 0.88 \frac{\text{Ca}_{\text{crit}}^{13/3}}{\ell^4} \log \left(\frac{\text{Ca}_{\text{crit}}}{\ell} \right). \quad (40)$$

The result in (40) indicates that the critical capillary number beyond which rupture is suppressed increases with increasing bubble length. This is qualitatively consistent with the experimental observations of Chen *et al.* [15]. However, we note that a quantitative comparison is not attempted due to the differing assumptions between our mathematical model and the experiments.

V. SUMMARY AND DISCUSSION

In this paper, we consider the unsteady motion of an inviscid bubble advancing at a constant speed in a cylindrical capillary tube, and subject to destabilizing van der Waals forces. Analytical expressions for the steady-state film profile $H_s(X; \beta)$, depending on the dimensionless van der Waals parameter β , are derived in the limiting cases of large and small β . A simplified numerical model is used to examine the growth of instabilities near the front or rear meniscus. Beginning from near the steady state, small perturbations are advected towards the rear of the bubble. Their amplitudes grow until a rupture instability occurs. Both the time-scale and length-scale of rupture is $O(1/\beta^2)$; notably, this indicates that for bubbles much shorter than this length, the instability travels into the rear before rupture occurs.

We also analyze how the Bretherton steady-state (with $\beta = 0$) is modified when attractive van der Waals forces become significant through a sudden transition from wetted to nonwetted substrates. Again, our asymptotic analysis demonstrates that if the bubble length is sufficiently small, then rupture is not expected to occur [cf. (40)].

As noted in Sec. IV B 3, while our asymptotic and numerical models agree qualitatively with the experimental observations of Chen *et al.* [15], a quantitative comparison is difficult due to the differing assumptions between our model and the experimental measurements. Our mathematical model describes a very long bubble of negligible viscosity in a circular tube, where the front and rear menisci do not interact with each other. On the other hand, the experiments measure a viscous drop of small finite length in a rectangular channel, where interaction between the front and the rear is inevitable. Thus, we highlight the need to (i) perform an experimental investigation of a bubble of negligible viscosity in a tube over a large range of bubble lengths; (ii) include viscous effects in our mathematical model to study the possible ways this can affect rupture dynamics; and (iii) develop a full numerical and analytical model which allows for arbitrary bubble lengths and shapes (and thus more complex interactions between the front and rear menisci). These considerations are the subject of ongoing work.

In the instances that rupture cannot be completely suppressed through modification of the flow velocity, there are other ways to delay its onset. For example, Matar & Kumar [34] show that both the addition of surfactants, as well as increased substrate flexibility will affect the time scale for rupture. Other studies have sought to understand the dynamics of thin-film flow on general curved surfaces [46–48], and for example, the recent work of [49] demonstrates that substrate curvature can prevent the classical Rayleigh-Taylor instability from occurring. It would be expected that similar considerations can be made for the situation of rupture instabilities. Given the particular importance and desirability of rupture in certain industrial applications (e.g., drug delivery [26]) we highlight the importance of developing a better understanding of the dynamics of bubble or droplet rupture in more general environments and geometries.

ACKNOWLEDGMENTS

Acknowledgements: The authors thank Jens Eggers and Isabelle Cantat for helpful conversations. We also gratefully acknowledge the Oxford-Princeton Collaborative Workshop Initiative for providing an opportunity for this collaborative work.

-
- [1] F. Fairbrother and A. E. Stubbs, Studies in Electro-endosmosis. Part VI. The “Bubble-tube” Method of Measurement, *J. Chem. Soc.* **1**, 527 (1935).
 - [2] G. I. Taylor, Deposition of a viscous fluid on the wall of a tube, *J. Fluid Mech.* **10**, 161 (1961).
 - [3] F. P. Bretherton, The motion of long bubbles in tubes, *J. Fluid Mech.* **10**, 166 (1961).
 - [4] H. L. Goldsmith and S. G. Mason, The flow of suspensions through tubes II. Single large bubbles, *J. Colloid Sci.* **18**, 237 (1963).
 - [5] L. W. Schwartz, H. M. Princen, and A. D. Kiss, On the motion of bubbles in capillary tubes, *J. Fluid Mech.* **172**, 259 (1986).
 - [6] H. Wong, C. J. Radke, and S. Morris, The motion of long bubbles in polygonal capillaries. Part 1. Thin films, *J. Fluid Mech.* **292**, 71 (1995).
 - [7] H. Wong, C. J. Radke, and S. Morris, The motion of long bubbles in polygonal capillaries. Part 2. Drag, fluid pressure and fluid flow, *J. Fluid Mech.* **292**, 95 (1995).
 - [8] C.-W. Park and G. M. Homsy, Two-phase displacement in Hele-Shaw cells: theory, *J. Fluid Mech.* **139**, 291 (1984).
 - [9] S. R. Hodges, O. E. Jensen, and J. M. Rallison, The motion of a viscous drop through a cylindrical tube, *J. Fluid Mech.* **501**, 279 (2004).
 - [10] E. Lac and J. D. Sherwood, Motion of a drop along the centreline of a capillary in a pressure-driven flow, *J. Fluid Mech.* **640**, 27 (2009).
 - [11] I. Cantat, Liquid meniscus friction on a wet plate: Bubbles, lamellae and foams, *Phys. Fluids* **25**, 031303 (2013).
 - [12] J.-D. Chen, Measuring the film thickness surrounding a bubble inside a capillary, *J. Colloid Interface Sci.* **109**, 341 (1986).
 - [13] K. Chaudhury, P. V. Acharya, and S. Chakraborty, Influence of disjoining pressure on the dynamics of steadily moving long bubbles inside narrow cylindrical capillaries, *Phys. Rev. E* **89**, 053002 (2014).
 - [14] G. F. Teletzke, H. T. Davis, and L. E. Scriven, Wetting hydrodynamics, *Rev. Phys. Appl.* **23**, 989 (1988).
 - [15] H. Chen, E. Dong, J. Li, and H. A. Stone, Adhesion of moving droplets in microchannels, *Appl. Phys. Lett.* **103**, 131605 (2013).
 - [16] D. Halpern and D. P. Gaver, Boundary element analysis of time-dependent motion of a semi-infinite bubble in a channel, *J. Comput. Phys.* **115**, 366 (1994).
 - [17] D. P. Gaver, D. Halpern, O. Jensen, and J. B. Grotberg, The steady motion of a semi-infinite bubble through a flexible-walled channel, *J. Fluid Mech.* **319**, 25 (1996).
 - [18] A. L. Hazel and M. Heil, The influence of gravity on the steady propagation of a semi-infinite bubble into a flexible channel, *Phys. Fluids* **20**, 092109 (2008).
 - [19] M. Heil, Airway closure: occluding liquid bridges in strongly buckled elastic tubes, *J. Biomech. Eng.-T. ASME* **121**, 487 (1999).
 - [20] M. Heil, Finite Reynolds number effects in the propagation of an air finger into a liquid-filled flexible-walled channel, *J. Fluid Mech.* **424**, 21 (2000).
 - [21] M. Heil, Finite Reynolds number effects in the Bretherton problem, *Phys. Fluids* **13**, 2517 (2001).
 - [22] C.-F. Tai, S. Bian, D. H. Y. Zheng, M. Filoche, and J. B. Grotberg, Numerical study of flow fields in an airway closure model, *J. Fluid Mech.* **677**, 483 (2011).
 - [23] H. Y. Erbil, A. L. Demirel, Y. Avci, and O. Mert, Transformation of a simple plastic into a superhydrophobic surface, *Science* **299**, 1377 (2003).
 - [24] P. Roach, N. J. Shirtcliffe, and M. I. Newton, Progress in superhydrophobic surface development, *Soft Matter* **4**, 224 (2008).
 - [25] K. Koch, B. Bhushan, Y. C. Jung, and W. Barthlott, Fabrication of artificial lotus leaves and significance

- of hierarchical structure for superhydrophobicity and low adhesion, *Soft Matter* **5**, 1386 (2009).
- [26] W. Arap, R. Pasqualini, and E. Ruoslahti, Cancer treatment by targeted drug delivery to tumor vasculature in a mouse model, *Science* **279**, 377 (1998).
 - [27] B. N. Blackstone, J. J. Willard, C. H. Lee, M. T. Nelson, R. T. Hart, J. J. Lannutti, and H. M. Powell, Plasma surface modification of electrospun fibers for adhesion-based cancer cell sorting, *Integr. Biol.* **4**, 1112 (2012).
 - [28] E. Ruckenstein and R. K. Jain, Spontaneous rupture of thin liquid films, *J. Chem. Soc., Faraday Trans. 2* **70**, 132 (1974).
 - [29] J. P. Burelbach, S. G. Bankoff, and S. H. Davis, Nonlinear stability of evaporating/condensing liquid films, *J. Fluid Mech.* **195**, 463 (1988).
 - [30] M. P. Ida and M. J. Miksis, Thin film rupture, *Appl. Math. Lett.* **9**, 35 (1996).
 - [31] T. P. Witelski and A. J. Bernoff, Dynamics of three-dimensional thin film rupture, *Physica D* **147**, 155 (2000).
 - [32] T. P. Witelski and A. J. Bernoff, Stability of self-similar solutions for van der Waals driven thin film rupture, *Phys. Fluids* **11**, 2443 (1999).
 - [33] W. W. Zhang and J. R. Lister, Similarity solutions for van der Waals rupture of a thin film on a solid substrate, *Phys. Fluids* **11**, 2454 (1999).
 - [34] O. K. Matar and S. Kumar, Rupture of a surfactant-covered thin liquid film on a flexible wall, *SIAM J. Appl. Math.* **64**, 2144 (2004).
 - [35] S. K. Kalpathy, L. F. Francis, and S. Kumar, Shear-induced suppression of rupture in two-layer thin liquid films, *J. Colloid Interface Sci.* **348**, 271 (2010).
 - [36] M. J. Davis, M. B. Gratton, and S. H. Davis, Suppressing van der Waals driven rupture through shear, *J. Fluid Mech.* **661**, 522 (2010).
 - [37] A. Oron, S. H. Davis, and S. G. Bankoff, Long-scale evolution of thin liquid films, *Rev. Mod. Phys.* **69**, 931 (1997).
 - [38] S. D. R. Wilson and A. F. Jones, The entry of a falling film into a pool and the air-entrainment problem, *J. Fluid Mech.* **128**, 219 (1983).
 - [39] P. Aussillous and D. Quéré, Quick deposition of a fluid on the wall of a tube, *Phys. Fluids* **12**, 2367 (2000).
 - [40] E. Klaseboer, R. Gupta, and R. Manica, An extended Bretherton model for long Taylor bubbles at moderate capillary numbers, *Phys. Fluids* **26**, 032107 (2014).
 - [41] N. Hammoud, *On Instabilities in Thin-Film Flows*, Ph.D. thesis, Princeton University (2016).
 - [42] W. Ren, P. H. Trinh, and W. E, On the distinguished limits of the Navier slip model of the moving contact line problem, *J. Fluid Mech.* **772**, 107 (2015).
 - [43] W. E. Schiesser, *The Numerical Method of Lines: Integration of Partial Differential Equations*, (Academic Press, 1991).
 - [44] T. Salez, J. D. McGraw, O. Bäumchen, K. Dalnoki-Veress, and E. Raphaël, Capillary-driven flow induced by a stepped perturbation atop a viscous film, *Phys. Fluids* **24**, 102111 (2012).
 - [45] H. A. Stone and C. Duprat, Model problems coupling elastic boundaries and viscous flows, in *Fluid-Structure Interactions in Low-Reynolds-Numbers Flows*, edited by C. Duprat and H. A. Stone (Royal Society of Chemistry, 2015).
 - [46] L. W. Schwartz and D. E. Weidner, Modeling of coating flows on curved surfaces, *J. Eng. Math.* **29**, 91 (1995).
 - [47] O. E. Jensen, The thin liquid lining of a weakly curved cylindrical tube, *J. Fluid Mech.* **331**, 373 (1997).
 - [48] P. D. Howell, Surface-tension-driven flow on a moving curved surface, *J. Eng. Math.* **45**, 283 (2003).
 - [49] P. H. Trinh, H. Kim, N. Hammoud, P. D. Howell, S. J. Chapman, and H. A. Stone, Curvature suppresses the Rayleigh-Taylor instability, *Phys. Fluids* **26**, 051704 (2014).